Volume 11
Number 23
7 December 2024
Pages 5801–6170

Materials Horizons

rsc.li/materials-horizons

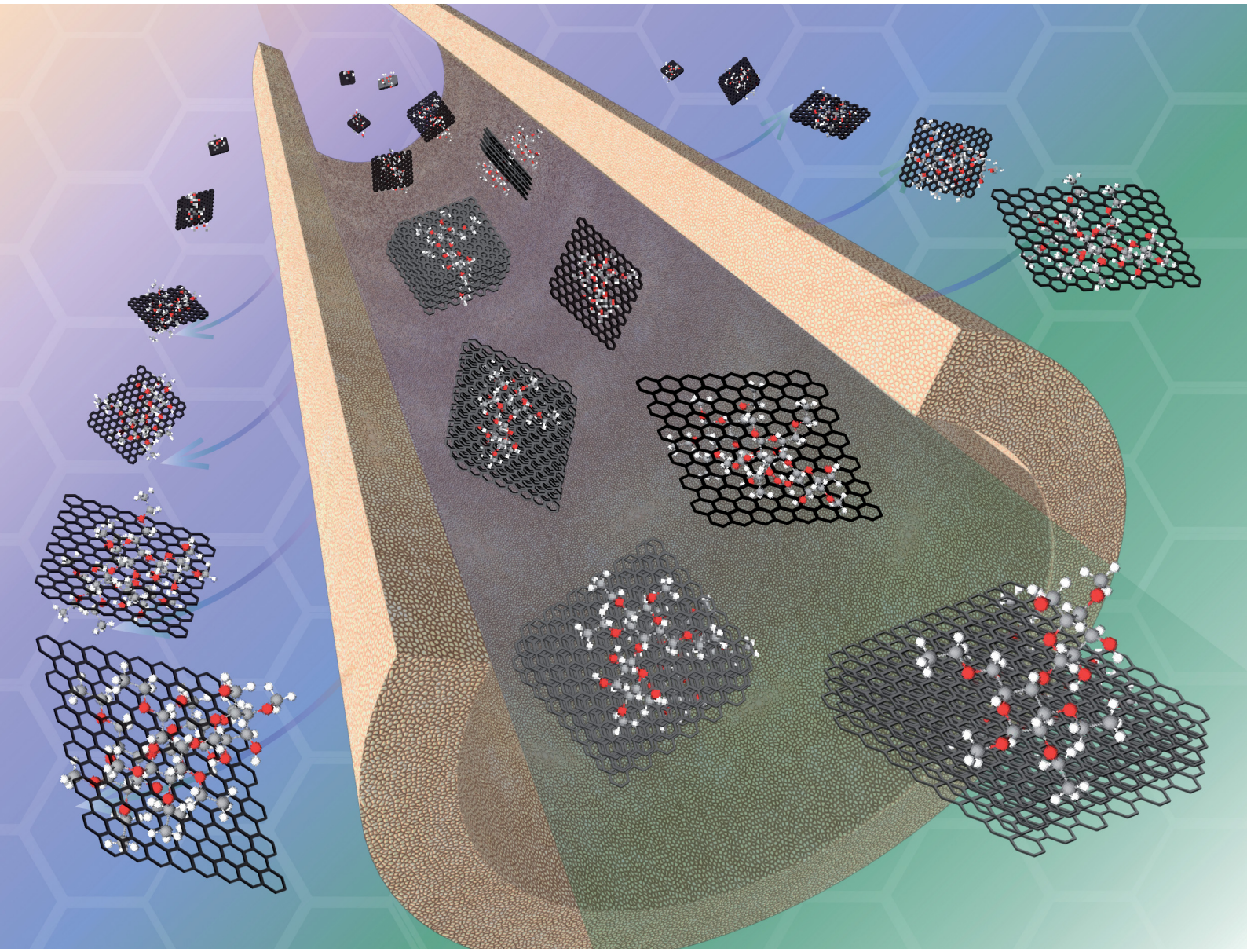

ISSN 2051-6347

ROYAL SOCIETY OF CHEMISTRY

COMMUNICATION
Mark C. Hersam *et al.*
Ultrahigh-throughput cross-flow filtration of solution-processed 2D materials enabled by porous ceramic membranes

10 YEARS ANNIVERSARY

Materials Horizons

ROYAL SOCIETY OF CHEMISTRY

COMMUNICATION

View Article Online
View Journal | View Issue

Cite this: *Mater. Horiz.*, 2024, **11**, 5960

Received 4th September 2024,
Accepted 30th September 2024

DOI: 10.1039/d4mh01205d

rsc.li/materials-horizons

Ultrahigh-throughput cross-flow filtration of solution-processed 2D materials enabled by porous ceramic membranes†

Santiago Diaz-Arauzo,[a] Julia R. Downing,[a] Daphne Tsai,[a] Jenna Trost,[b] Janan Hui,[c] Kevin Donahue,[d] Nick Antonopoulos,[d] Lindsay E. Chaney,[a] Jennifer B. Dunn [b] and Mark C. Hersam *[ace]

Printed electronics is a disruptive technology in multiple applications including environmental and biological sensors, flexible displays, and wearable diagnostic devices. With superlative electronic, optical, mechanical, and chemical properties, two-dimensional (2D) materials are promising candidates for printable electronic inks. While liquid-phase exfoliation (LPE) methods can produce electronic-grade 2D materials, conventional batch separation processes typically rely on centrifugation, which requires significant time and effort to remove incompletely exfoliated bulk powders, hindering the scale-up of 2D ink manufacturing. While cross-flow filtration (CFF) has emerged as a promising continuous flow separation method for solution-processed 2D nanosheets, previously demonstrated polymer CFF membranes necessitate low 2D nanosheet concentrations to avoid fouling, which ultimately limits mass throughput. Here, we demonstrate a fully flow-based, exfoliation-to-ink system for electronic-grade 2D materials using an integrated cross-flow separation and concentration system. To overcome the relatively low-throughput processing concentrations of incumbent polymer CFF membranes, we employ porous ceramic CFF membranes that are tolerant to 10-fold higher nanosheet concentrations and flow rates without compromising separation efficiency. Furthermore, we demonstrate a concentration method *via* cross-flow ultrafiltration, where the retentate can be directly formulated into printable inks with electronic-grade performance that meets or exceeds centrifugally produced inks. Life cycle assessment and technoeconomic analysis quantitatively confirm the advantages of ceramic *versus* polymer CFF membranes including reductions of 97%, 96%, 94%, and 93% for greenhouse gas emissions, water consumption, fossil fuel consumption, and specific production costs, respectively. Overall, this work presents an environmentally sustainable and cost-effective solution for the fabrication, separation, and printing of electronic-grade 2D materials.

New concepts

Printed electronics is a disruptive technology in multiple applications including flexible displays, environmental sensors, and wearable diagnostic devices. With superlative electronic, mechanical, and chemical properties, two-dimensional (2D) materials are promising candidates for printable electronic inks. While liquid-phase exfoliation methods can produce electronic-grade 2D materials, conventional separation processes rely on batch centrifugation, which hinders the scale-up of 2D ink manufacturing. To avoid batch centrifugation, cross-flow filtration (CFF) provides a continuous-flow separation method for solution-processed 2D nanosheets, but previously demonstrated polymer CFF membranes necessitate low 2D nanosheet concentrations to avoid fouling, which ultimately limits mass throughput. Here, we demonstrate a fully flow-based, exfoliation-to-ink process for electronic-grade 2D materials using integrated cross-flow separation and concentration. To overcome the relatively low-throughput of incumbent polymer CFF membranes, we employ porous ceramic CFF membranes that are tolerant to 10-fold higher nanosheet concentrations and flow rates without compromising separation efficiency. Life cycle assessment and technoeconomic analysis quantitatively confirm the advantages of ceramic *versus* polymer CFF membranes including reductions of greenhouse gas emissions, water consumption, fossil fuel consumption, and specific production costs by >90%. Overall, this work presents an environmentally sustainable and cost-effective solution for the fabrication, separation, and printing of electronic-grade 2D materials.

[a] *Department of Materials Science and Engineering, Northwestern University, Evanston, Illinois 60208, USA. E-mail: m-hersam@northwestern.edu*
[b] *Department of Chemical and Biological Engineering, Northwestern University, Evanston, Illinois 60208, USA*
[c] *Department of Chemistry, Northwestern University, Evanston, Illinois 60208, USA*
[d] *ALSYS USA, CeraMem, Waltham, Massachusetts 02453, USA*
[e] *Department of Electrical and Computer Engineering, Northwestern University, Evanston, Illinois 60208, USA*

† Electronic supplementary information (ESI) available. See DOI: https://doi.org/10.1039/d4mh01205d

Introduction

The increasing demand for two-dimensional (2D) materials has inspired efforts to realize industrial-scale production methods, where the highest processing throughputs have been achieved using solution-based processing.[1] Since the thickness and lateral size of 2D materials have significant effects on their electronic properties, it is critical to achieve high monodispersity in these parameters, which has traditionally been achieved through centrifugation-based batch separation following liquid-phase exfoliation (LPE).[2–4] However, since batch processing introduces bottlenecks into scalable manufacturing, it is of high interest to identify and demonstrate alternative continuous-flow separation methods. Flow-based separation techniques commonly rely on membrane-based processes, such as reverse osmosis, dead-end filtration, and cross-flow filtration (CFF), which are ubiquitous in the fields of biotechnology, pharmaceuticals, and chemical engineering.[5–8] When translating these techniques to the field of 2D materials, relatively low exfoliation yields imply the need to isolate the smallest nanosheets that make up a miniscule fraction of the total input stream and are often orders of magnitude smaller than poorly exfoliated bulk powders, which results in rapid fouling of membrane-based processes, thus hindering their deployment in industrial-scale production of electronic-grade 2D materials.[9]

Graphene is the prototypical 2D material,[10] and solution-processed graphene nanosheets have already been successfully deployed in composites, printable conductive inks, and electrode materials.[11,12] As these applications continue to grow on the industrial scale, graphene demand is rapidly approaching 1 tonne year^{-1}.[9] Despite this growing demand, the environmental impact of graphene manufacturing is largely unexplored,[13] particularly for post-exfoliation separation techniques that are required for reliable downstream performance. Ultimately, widespread commercialization of graphene production will require consistent quality, low cost, reproducibility, processability, and safety at all steps of the manufacturing pipeline.[9] Environmental impacts will also become increasingly important when production levels exceed 1 tonne year^{-1}.[14]

Achieving mass production of electronic-grade graphene nanosheets is challenging due to the need to achieve high monodispersity in structural features (*e.g.*, thickness and lateral size) while maintaining low defect and impurity levels.[15] Typically, industrial-scale production of graphene is accomplished using LPE methods. This approach entails the suspension of bulk graphite particles in a liquid solvent, often with surfactants or stabilizing polymers, after which exfoliation is achieved *via* mechanical agitation that induces cavitation-induced shearing.[16] While the mechanical agitation is often performed in a batch processes (*e.g.*, sonication), LPE has also been implemented using continuous-flow methods such as shear mixing or wet jet milling.[17]

Since the exfoliation yield down to nanoscale thicknesses for LPE is typically on the order of 1%, it is essential to employ a post-exfoliation separation strategy to remove the poorly exfoliated bulk powders. For electonic-grade graphene nanosheets, this post-exfoliation separation is almost exclusively achieved using batch centrifugation.[16,17] During centrifugation, the poorly exfoliated bulk powders rapidly sediment, allowing the desired nanosheets to be isolated into the supernatant. The supernatant can then be powderized by removing the solvent using batch methods such as vacuum filtration or rotary evaporation.[18] Overall, these post-exfoliation steps are effective at the lab-scale, but become bottlenecks to scalable manufacturing due to their labor-intensive and energy-intensive batch processing.[19]

In contrast, membrane-based separation is an appealing flow-based alternative for post-exfoliation processing due to its low capital equipment cost, continuous-flow operation, and lower energy consumption.[19,20] However, the fact that up to 99% of the output from LPE consists of relatively large, poorly exfoliated particles, membranes experience rapid fouling for LPE separations, which undermines the advantages of this methodology.[21,22]

Cross-flow filtration (CFF) is a membrane-based process where colloidal suspensions pass tangentially across a membrane, thereby minimizing the build-up of a filter cake on the membrane surface. The CFF process allows for extended filtration times and higher feed concentrations compared with dead-end filtration because the turbulent flow across the membrane surface mitigates fouling.[21] CFF is categorized by the pore size of the membrane, where cross-flow nanofiltration, ultrafiltration, and microfiltration feature pore sizes of 0.1–10 nm, 10–100 nm, and 100–10 000 nm, respectively. Traditionally, cross-flow microfiltration (CF-MF) processes isolate the desired product in the retentate (*i.e.*, the colloidal dispersion that does not travel through the membrane) and the permeate is subsequently discarded.[23–28] In these cases, the filtration is performed at relatively low feed concentrations, requiring multiple trials to obtain sufficient quantities of material required for commercial applications. CF-MF typically employs polymer membranes (*e.g.*, polysulfone, polyethersulfone, or polycarbonate), which have relatively low pressure ratings that limit the use of high cross-flow velocities. While these conditions are acceptable for cases where the feed stream has a low percentage of impurities that need to be removed, LPE dispersions present the opposite condition where the nanosheets to be retained are the minority species. Therefore, CF-MF for LPE dispersions needs to be run under conditions where the desired nanosheets are isolated in the permeate stream and the retentate stream is discarded or recycled.

Since most nanomaterial separation problems exist in this unconventional regime for CF-MF, CF-MF has only been demonstrated for nanomaterials in the limited cases when the standard conditions have been met (*i.e.*, removing minority impurity species through the permeate from a dispersion that is already enriched with the targeted nanomaterial).[23–27] In these cases, relatively low concentrations and flow rates have been employed, which has limited overall processing throughput to the lab-scale.[28,29] Recently, we demonstrated conditions under which CF-MF can be employed for LPE graphene

nanosheet separation by employing CF-MF in the unconventional regime (*i.e.*, isolating graphene nanosheets in the permeate stream). However, this proof-of-concept study employed hollow fiber polysulfone membranes, which required low concentration feed streams to avoid fouling, thus still limiting throughput to the lab-scale.[19] Moreover, while CF-MF allowed the isolation of electronic-grade graphene nanosheets, post-separation flocculation and vacuum filtration were required to powderize the graphene nanosheets so that they could then be redispersed into printable ink formulations, implying that batch processing steps were not completely eliminated. Likewise, other attempts to scale-up electronic-grade graphene ink production have relied on centrifugation,[30–33] and thus a fully integrated continuous-flow processing scheme for 2D electronic inks has not yet been achieved.

Here, we integrate CF-MF and cross-flow ultrafiltration (CF-UF) to achieve a fully integrated continuous-flow processing system for electronic-grade graphene inks. In this integrated system, the graphene nanosheets are separated from the input LPE dispersion in the CF-MF permeate stream, which is then fed into CF-UF. In the CF-UF stage, the solvent is removed through the permeate stream, leading to concentration of the CF-UF retentate stream up to levels suitable for printable inks, thereby eliminating any batch processing. A key innovation in this continuous-flow processing system is the use of porous ceramic CFF membranes in place of polymer CFF membranes. The improved mechanical integrity of the ceramic CFF membranes allow the input flow rate to be substantially increased, which minimizes fouling even at high input concentrations, ultimately allowing 10-fold higher nanosheet concentrations and flow rates without compromising filtration efficiency. The resulting printable graphene inks show superlative electronic properties that meet or exceed incumbent electronic-grade graphene inks. Moreover, life cycle assessment and techno-economic analysis confirm that the higher flow rates and concentrations enabled by ceramic *versus* polymer CFF membranes result in reductions of 97%, 96%, 94%, and 93% for greenhouse gas emissions, water consumption, fossil fuel consumption, and specific production costs, respectively. Importantly, the generality of this methodology implies that it can be broadly applied to other solution-processed 2D materials, thus enabling environmentally sustainable and cost-effective deployment of 2D materials in industrial-scale applications.

Experimental

Materials

Graphite powder (MICRO 450, #27391) was purchased from Asbury Carbons (Port Huron, MI). Ethanol was manufactured by Decon Laboratories (King of Prussia, PA) and purchased from Fisher Scientific (Waltham, MA, Catalog no. 04-355-223). Ethyl cellulose (4 cP, 5% in 80 : 20 toluene : ethanol, #200646) was purchased from MilliporeSigma. For polymer membrane control studies, polysulfone (PS) hollow fiber cartridges from Cytiva (Marlborough, MA) with pore sizes of 0.65 μm (#CFP-6-D-5A) were used.

Liquid-phase exfoliation

A dispersion of 82 g of ethyl cellulose (EC) in 7570 mL of ethanol (≈1% w/v) was prepared by mixing the solution using a magnetic stir bar overnight. 893 g of graphite powder (≈12% w/v) was then poured into the container and stirred using a magnetic stir bar at 700 rpm for 30 min while heating at 45 °C. The resulting dispersion was transferred into a holding vessel for a Starburst Labo wet jet milling instrument (Sugino Corporation, Itasca, IL). The wet jet milling instrument was operated at 200 MPa for 120 min to achieve 10 passes through the system.

Cross-flow filtration

CFF experiments were performed using a cross-flow filtration system constructed in-house. A 2.5-gallon tank (Ace Roto-Mold, McMaster Carr #471870) was affixed to the top of a mobile cart. Polyethylene pump tubing (Everbilt, Cole Parmer #301762) was run from the base of the tank through a peristaltic feed pump (Cole-Parmer, Model #77111-71). At the discharge of the feed pump, polyethylene tubing was plumbed to the entry of the Al_2O_3 microfiltration membrane element (pore size = 1000 nm, Kleansep). Additional polyethylene tubing connected the retentate port to the holding tank to recirculate the dispersion for successive passes through CFF. The permeate stream was split from the retentate, wherein polyethylene tubing was routed into a separate container to collect the permeate dispersion. A digital pressure monitor (Spectrum Labs, Model no. 900-1607) was used to collect pressure readings from pressure transducers at the feed, permeate, and retentate ports on the microfiltration apparatus.

Thereafter, a peristaltic pump (MasterFlex, 07528-10) drove the microfiltration permeate dispersion into the feed port of the Al_2O_3 ultrafiltration membrane element (pore size = 100 nm, Ceramem). The retentate from the ultrafiltration element was concentrated by removing ethanol and ethyl cellulose at the permeate port until the final volume of the ultrafiltration retentate was ≈5% of the original feed volume. Barbed and tri-clamp adapters, reducers, and fittings were installed throughout the flow path to minimize the presence of leaks.

Membrane regeneration procedure

Between experiments, both water and ethanol were pumped at 6.0 GPM in standard and backflush modes to flush away retentate particles physiosorbed to the membrane surface. The solvent was then drained from the system. Subsequently, exfoliated dispersion was mixed in the tank with diluent ethanol by recirculating the mixed solution for 5 min to obtain a constant feed concentration of 1 g L^{-1} for the polymer membrane studies and a feed concentration of 10 g L^{-1} for the ceramic membrane studies. Across the CFF experiments, the feed flow rate was modulated from 3.03–22.7 L min^{-1} for CF-MF, and the feed flow rate for CF-UF was modulated from 0 – 1.68 L min^{-1}. The channel-flow velocity was regulated by

modifying the flow rate and was determined by dividing the flow rate with the channel area.

Preparation of printable inks

To prepare inks for aerosol jet printing, the concentrated CF-UF retentate containing graphene/EC was combined with terpineol at a solvent volume ratio of 90 : 10 with a powder concentration of 10 g L^{-1}. The ink was then fed through a nylon Whatman syringe filter with a pore size of 3.1 μm prior to printing. Aerosol jet printing (AJP) experiments were carried out using a commercial aerosol jet printer (Aerosol Jet 200, Optomec) equipped with a 150 μm nozzle, following previous studies with graphene inks.[33,34] The platen temperature was set to 60 °C, and the bath temperature was set to 30 °C. The inks were printed onto an ozone plasma-cleaned glass substrate using a print speed of 5 mm s^{-1}, with nitrogen sheath flow set to 60 sccm, a carrier gas flow rate of 15–22 sccm, and an atomization current of 0.354 mA. The specimens were heated in a box furnace at 350 °C for 30 min after printing to pyrolyze the EC binder.

Life cycle assessment and technoeconomic analysis

Life cycle assessment (LCA) was based on ISO 14040/44 standards.[35,36] Technoeconomic analysis (TEA) evaluated the energy, material, and water usage as well as the cost effectiveness of each process through a comprehensive analysis of material and energy flows and an annualized cost methodology.[37] The functional unit used for comparison between the two processes was 1 L of graphene ink. To convert the LCA/TEA impacts from graphene produced in grams (g) to graphene ink in liters (L), we assumed an impact factor of 10 based on the required concentration of graphene required to produce 1 L of ink (10 g L^{-1}) as summarized in eqn (1):

$$\frac{1}{\text{L of graphene ink}} = \frac{1}{\text{g of graphene}} \times \frac{10\text{ g of graphene}}{\text{L of ink}} \quad (1)$$

All costs were defined using the US Dollar ($) in 2023. The specific production cost of graphene ink (C_P, $ L^{-1}) was determined through an annualized cost approach as shown in eqn (2):

$$C_p = \frac{C_{AC} + C_{O\&M}}{T} + C_M \quad (2)$$

The annualized capital costs (C_{AC}) were calculated based on the process lifetime (n, 20 years) and discount rate (r) as shown in eqn (3):

$$C_{AC} = C_c \times \frac{r \times (1+r)^n}{(1+r)^n - 1} \quad (3)$$

The operating and maintenance expenses ($C_{O\&M}$) for each process include the total costs from labor, electricity, and consumables. The capital costs (C_C) of the two processes were estimated by the equipment list prices. The material costs (C_M) were defined as the costs from the raw materials, mainly graphene, ethanol, ethyl cellulose, and terpineol in comparison to the functional unit of 1 L of graphene ink, where T is throughput of graphene ink. We empirically observed that ceramic membranes can operate for 50–70 cycles and thus assumed that 10 filters are needed on a yearly basis for ~7000 runs. Complete information and assumptions regarding all LCA/TEA parameters are provided in the ESI.†

Results and discussion

Process overview

The flow-based manufacturing process, shown in Fig. 1(a), begins with thorough mixing of graphite and ethyl cellulose in ethanol to achieve a homogeneous dispersion. The resulting dispersion is then introduced into a wet jet milling apparatus for LPE, producing graphene nanosheets with a conversion rate of 1–3%. To separate the desired graphene nanosheets from the poorly exfoliated bulk powder, CF-MF is employed using ceramic membranes with micron-sized pores. A detailed discussion of the flow characteristics and membrane properties are provided in the ESI.† The ceramic membranes were placed into a stainless-steel support as shown in Fig. 1(b). A 2.5-gallon reservoir tank was installed on the upper shelf of the cart to hold the input LPE dispersion. Commercially available pump tubing and adapters were fitted to create a closed-loop recirculation pathway for the graphene dispersions.

A high-flow (≈11 GPM) peristaltic pump transports the feed LPE dispersion from the tank into the input stream for CF-MF. A secondary small-scale (<0.5 GPM) peristaltic pump promotes cross-flow filtration by introducing a pumping force on the permeate steam perpendicular to the primary flow direction inside the ceramic membrane. The retentate stream is pumped back into the reservoir tank and recirculated for subsequent passes through CF-MF.

After CF-MF, the secondary small-scale peristaltic pump transports the CF-MF permeate into the input stream for CF-UF as shown in Fig. 1(b). A separate small-scale peristaltic pump is used on the permeate side of the nanometer-sized CF-UF membrane to promote ethanol and EC removal, thus concentrating the graphene nanosheet dispersion in the CF-UF retentate stream. This CF-UF process functions similarly to conventional demonstrations of CFF in the nanomaterials literature, which purify or concentrate the target material in the retentate.[27,28] The integrated CF-MF/CF-UF system was operated continuously until the ultrafiltration retentate was concentrated by a factor of 20, meaning that the CF-MF permeate was concentrated from 0.5 g L^{-1} to 10 g L^{-1}.

Typical protocols employed for the isolation and separation of 2D materials necessitate a solid–liquid evaporation step to achieve ink formulations, incorporating methodologies such as rotary evaporation,[17] flocculation,[31] and solvent exchange.[34] Instead of pursuing these conventional batch processes, we pursued a direct ink concentration approach using CF-UF. CF-UF directly concentrates the graphene nanosheet dispersion in the retentate stream, which is then combined with terpineol to attain an ink formulation amenable for aerosol jet printing (AJP). Leveraging the versatility of AJP, we printed multiple,

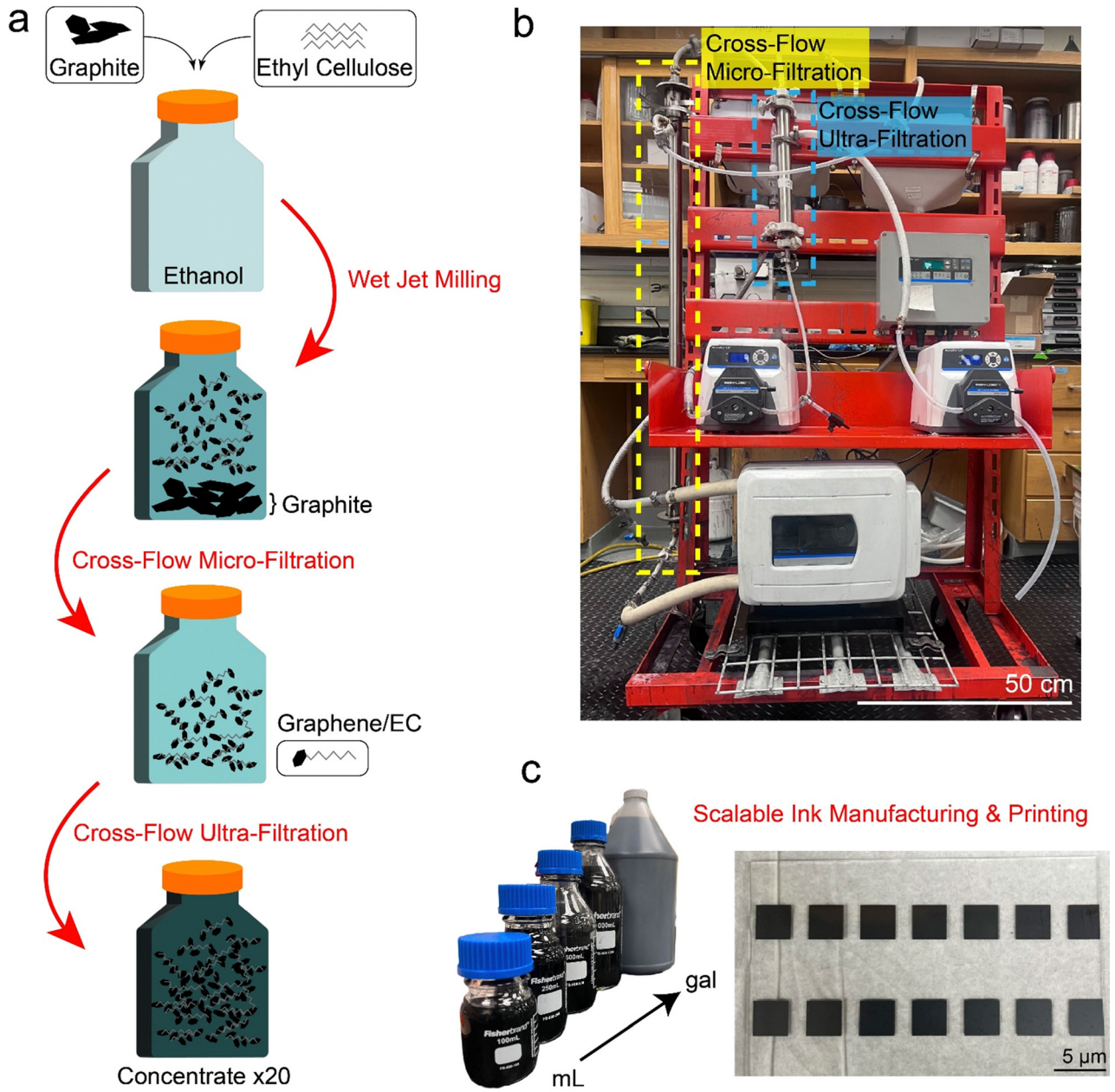

Fig. 1 Gallon-scale manufacturing of graphene inks. (a) Process overview for the scalable production of graphene inks *via* cross-flow filtration (CFF). Ethyl cellulose (EC) and graphite are dispersed in the presence of ethanol and then fed into a wet jet mill for liquid phase exfoliation (LPE). The polydisperse sample, containing partially-exfoliated graphite and well-exfoliated graphene, is processed *via* microfiltration to remove graphite. Subsequently, the graphene/EC/ethanol dispersion is concentrated *via* ultrafiltration by a factor of 20. (b) Photograph depicting the integrated CFF process, with microfiltration highlighted in yellow and ultrafiltration highlighted in blue. (c) Through the incorporation of ceramic membranes in CFF, the resulting high-throughput, continuous-flow process enables gallon-scale production of electronic-grade printable graphene inks.

high-resolution films using this concentrated ink, showcasing the scalability and efficiency of our flow-based approach to the gallon-scale (Fig. 1(c)).

Process characteristics of cross-flow filtration

In both CF-MF and CF-UF, the process fundamentally differs from traditional dead-end filtration in that the dispersion travels tangentially along the membrane surface rather than directly through it. The main advantage of this process is that this flow pattern minimizes the formation of a filter cake, which rapidly inhibits the filtration efficiency. In our process, the feed dispersion for CF-MF is driven by a large-scale peristaltic pump and passed through channels containing a distribution of pores (Fig. 2(a) and (b)). The dispersion travels tangentially along the membrane surface (“channel flow”), and particles smaller than the pore size travel perpendicular to the channel surface into the permeate (“permeate flow”). The larger particles that do travel through the membrane pores are

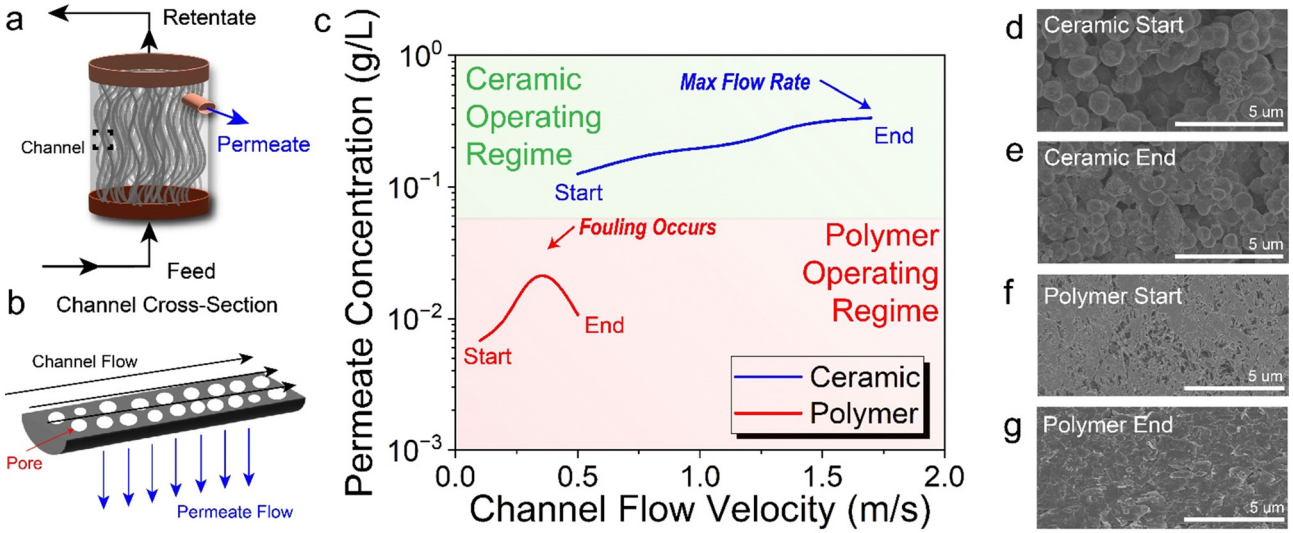

Fig. 2 Cross-flow filtration. (a) Schematic diagram of the cross-flow filtration (CFF) process, depicting the three process streams: feed, retentate, and permeate. (b) Flow pattern of the process streams in an individual channel cross-section. (c) Permeate concentration plotted with respect to channel flow velocity (CFV). (d) and (e) High CFV dislodges fouling particles and result in a clean ceramic membrane surface, as shown in scanning electron microscopy (SEM) images at the start and end of CFF processing, respectively. (f) and (g) Polymer membranes have limited mechanical durability, and thus can only tolerate low CFV before fouling occurs, as illustrated by SEM images at the start and end of CFF processing, respectively.

retained as the "retentate flow" and recirculated back into the filter. Throughout this process, the underlying driving force for filtration is the transmembrane pressure (TMP, eqn (4)):

$$\text{Transmembrane Pressure (TMP)} = \frac{(P_F + P_R)}{2} - P_P \qquad (4)$$

where the first term corresponds to the average of the feed pressure (P_F) and the retentate pressure (P_R), and the second term corresponds to the permeate pressure (P_P). Nominally, membranes are rated for a range of transmembrane pressures based on the constituent material. For example, polysulfone membranes are rated up to 10 PSI, whereas the more mechanically robust ceramic membranes are rated upwards of 140 PSI. As a result, polymer membranes are typically implemented in filtration processes at low flow rates and low transmembrane pressures.

Membrane selection is paramount to the successful filtration of the selected material. Specifically, careful consideration must be given to the membrane material, geometry, surface area, number of channels, porosity, pore size, and process characteristics. These parameters all contribute to the membrane flux (J) that is described by eqn (5):[38]

$$J = \frac{\text{TMP}}{\mu(R_m + R_c)} \qquad (5)$$

Flux is reported in units of L m^{-2} h^{-1}, where μ corresponds to the viscosity of the dispersion, TMP is the transmembrane pressure, and R_m and R_c correspond to the internal membrane resistance and cake resistance from particulate buildup. In an effort to maximize process throughput, we focused on enabling high flow rates and high dispersion concentrations. Therefore, the critical process control parameters are transmembrane pressure, membrane material, and channel flow velocity (CFV), which are tabulated in the ESI.† In order to ensure consistently high membrane flux, we designed our system for high channel flow rate to minimize the possibility of cake buildup even at high concentrations. In this regard, polymer membranes are suboptimal since their transmembrane pressure operating window falls well below the necessary flow rates to prevent cake buildup at high concentrations. Consequently, ceramic membranes became the primary focus of this work.

In order to quantitatively evaluate ceramic membranes for CFF of LPE graphene dispersions, we performed a series of experiments to collect and measure the permeate concentration at various CFVs (Fig. 2(c)). For the polymer membrane studies, we followed the same experimental procedure from our previous report[19] using a feed concentration of 1 g L^{-1}. In contrast, the high flow rates enabled by ceramic membranes allowed 10-fold higher feed concentrations of 10 g L^{-1}. In the case of the polymer membrane, as we began to ramp the channel flow, we observed a corresponding increase in the permeate concentration. However, after reaching a CFV of 0.35 m s^{-1}, membrane fouling caused the permeate concentration to decrease before ultimately resuling in complete clogging. Although we attempted to recover the polymer membrane through exhaustive cleaning procedures, the fouling proved to be irreversible for the polymer membrane (Fig. S1, ESI†). Alternatively, the ceramic membrane experiment began at a higher CFV of 0.5 m s^{-1}. The CFV was similarly ramped, and the permeate dispersions were collected for characterization. We found that increases in CFV improved the filtration performance as indicated by the increased permeate concentrations. Impressively, the ceramic membranes performed well with no evidence for fouling up to the maximum flow rate of the peristaltic feed pump.

To evaluate the degree of membrane fouling, the membrane surface was imaged with scanning electron microscopy (SEM) before and after CFF. The membrane surface was coated with a 10 nm layer of OsO_4 in order to minimize charging during SEM imaging. SEM images of the ceramic membrane surface revealed no detectable changes before and after CFF, thus confirming the absence of fouling (Fig. 2(d) and (e)). In contrast, the initially porous microstructure on the exterior surface of the polymer membrane (Fig. 2(f)) was obstructed with a dense layer of graphitic particles following CFF (Fig. 2(g)). Evidently, the ability of the mechanically durable ceramic membrane to withstand high CFVs leads to minimal fouling even for high feed concentrations.

Material properties of graphene following cross-flow filtration

To evaluate our flow-based process in comparison to batch-based processes like centrifugation,[17,30–33] extensive materials characterization of the resulting graphene nanosheets was performed using SEM, atomic force microscopy (AFM), Raman spectroscopy, and optical microscopy. In particular, we evaluated two classes of CFF dispersions side-by-side. First, the CF-MF feed and retentate dispersions containing mixed populations of graphene nanosheets and graphite particles were transferred from the CFF reservoir tank to a rotary evaporator in order to remove the solvent. The collected graphitic solids were then redispersed and formulated into the first ink. Secondly, the CF-UF retentate stream containing concentrated graphene nanosheets was sampled directly as the second ink. Both the mixed CF-MF feed/retentate and the CF-UF retentate ink were drop-cast onto plasma-cleaned glass substrates to form percolating films. The stabilizing EC was then removed by thermal decomposition, similar to previous reports on EC decomposition.[19,31–34,39,40] SEM imaging (Fig. 3(a)–(c)) reveals clear differences between the two inks: the CF-MF feed/retentate (Fig. 3(a) and (b)) contains micron-sized graphite particles throughout the film, whereas the CF-UF retentate (Fig. 3(c)) exclusively contains graphene nanosheets.

AFM was used to characterize the drop-casted CF-UF retentate to quantify the lateral size and thickness of the graphene nanosheets (Fig. 3(d)). From a population (n = 300) of graphene nanosheets, we found an average lateral size (square root of flake area) $\langle\sqrt{A_{\text{flake}}}\rangle$ = 452.74 nm and average thickness $\langle t_{\text{flake}}\rangle$ = 2.86 nm (Fig. 3(e) and (f)). In comparison to graphene nanosheets prepared by polymer membrane CFF[19] and related studies on electronic-grade graphene nanosheets,[17,30] the flake thickness is comparable and the flake lateral size is marginally greater, which is consistent with the marginally larger pore size of the ceramic membranes compared to the polymer membranes.

Raman spectroscopy was performed as an additional quality control measure (Fig. S3, ESI†). Graphene quality can be assessed using the intensity ratio between the D and G peaks (I_D/I_G), where the D peak stems from the presence of structural defects such as vacancies, lattice disorder, and edge defects,[41,42] and the G peak corresponds to the graphitic peak resulting from the sp^2 carbon atoms.[41] The CF-UF retentate showed an I_D/I_G ratio of approximately 0.28, and the G, D, D′, and 2D peaks were found at approximately 1350 cm^{-1}, 1580 cm^{-1}, 1620 cm^{-1}, and 2700 cm^{-1}, respectively, which is consistent with electronic-grade graphene nanosheets.[19,43] Additionally, the position of the G peak and the ratio of the G and 2D peaks (I_G/I_{2D}) serve as indicators of the number of graphene layers. The G peak position at $\approx$1580 cm^{-1} and the I_G/I_{2D} ratio of approximately 2.08 suggest a film composed of few-layered graphene flakes, which agrees with the AFM thickness data and a previous report on graphene produced from polymer CFF.[19]

To confirm the electronic properties of the graphene nanosheets, the concentrated CF-UF retentate was combined with terpineol to produce an ink suitable for AJP. Before AJP, the graphene inks were filtered through a 3.1 μm membrane, which is a standard practice for AJP with colloidal inks.[19,34] The resulting ink was ultrasonically atomized using a frequency of $\approx$1 MHz and printed onto glass slides using conditions derived from previous reports of AJP graphene inks processed *via* batch centrifugation.[34] After printing, the substrates were thermally treated to remove the stabilizing EC, similar to the drop-casted samples. Following this treatment, well-defined 20 μm wide lines were observed with optical microscopy, while SEM confirmed the formation of a percolating network of tightly packed graphene nanosheets (Fig. 3(g)).

The electronic properties of the printed graphene patterns were evaluated using four-point probe charge transport measurements.[43] The film conductivity was confirmed to be 4×10^4 S m^{-1} (Fig. 3(h)), which is competitive with the electronic-grade graphene produced with polymer membrane CFF[19] and conventional centrifugally processed graphene inks in blade-coated,[17] inkjet-printed,[40] and screen-printed[39] films. Additionally, we found that the viscosity of the graphene ink remained consistent throughout the manufacturing process, which is important to ensure process stability, printing performance, and batch-to-batch consistency (Fig. S4, ESI†).[44] In addition, the graphene ink produced from the CF-UF retentate retained shear-thinning behavior consistent with conventionally manufactured graphene inks from centrifugation (Fig. S5, ESI†).[39,40]

To demonstrate the advantage of ceramic membrane CFF on manufacturing throughput, the mass throughput and feed concentration were compared against previous nanomaterial CFF reports (Fig. 3(i) and Table S3, ESI†). Here, we define mass throughput as the product of volumetric throughput and the mass concentration of solid particles (Fig. S6 and Table S3, ESI†). It is worth noting that most of these demonstrations are operated in the conventional mode of CFF, where the permeate is discarded and the retentate is further processed. While our previous demonstration of CFF-processed graphene with polymer membranes showed a high volumetric throughput of $\approx$15 L $hour^{-1}$, the feed concentration was below 1 g L^{-1}, significantly limiting the mass throughput.[19] In contrast, ceramic membrane CFF not only enables a higher volumetric throughput ($\approx$ 100 L $hour^{-1}$) but also higher feed concentrations, resulting in a 10-fold increase in mass throughput. Additionally, the elimination of centrifugation and rotary

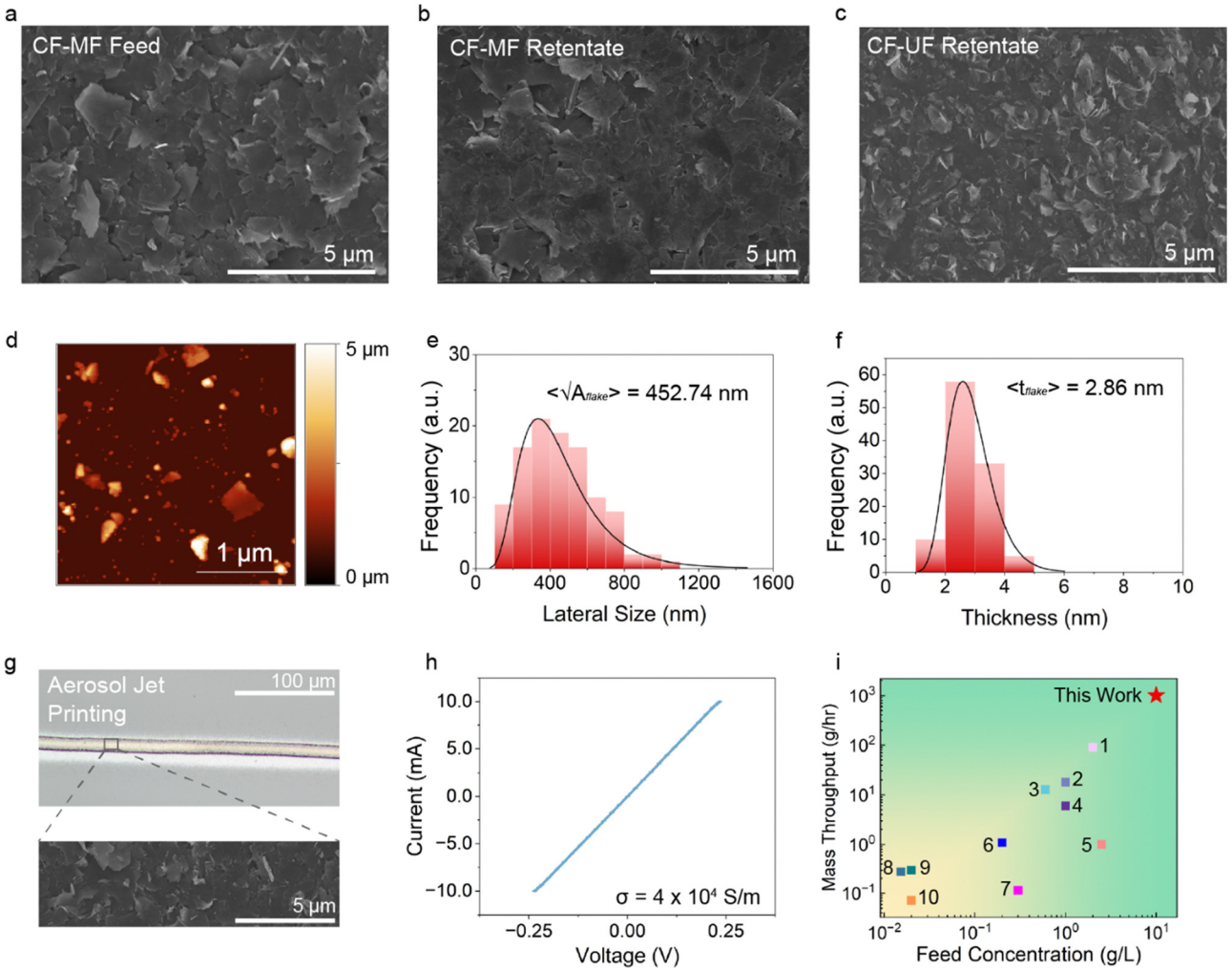

Fig. 3 Material properties of graphene nanosheets produced using cross-flow filtration. (a) Scanning electron microscopy (SEM) image of drop-casted CF-MF feed dispersions, showing the presence of large graphite flakes. (b) SEM image of the drop-casted CF-MF retentate dispersions, which show a similar morphology to the feed dispersion. (c) SEM image of the drop-casted CF-UF retentate dispersions, showing the formation of a smooth film comprised of graphene nanosheets. (d) Atomic force microscopy (AFM) of the CF-UF retentate sample, again confirming the presence of graphene nanosheets. (e) and (f) AFM histograms (n = 300) of the drop-casted CF-UF retentate sample, showing log-normal distributions of lateral size and flake thickness, respectively. (g) Optical microscopy image (top) and SEM image (bottom) of aerosol jet printed (AJP) features showing smooth edges and well-defined graphene nanosheet morphology. (h) Four-point probe charge transport characterization of aerosol jet printed graphene confirms ohmic current–voltage behavior with an electrical conductivity of 4×10^4 S m^{-1}. (i) Mass throughput and feed concentration in this work show significant improvements compared to previously reported nanomaterial cross-flow filtration processes. The references are detailed in Table S3 of the ESI.†

evaporation steps significantly reduces energy consumption, which will be further discussed in the following section. In summary, this comparison underscores the value of ceramic membrane CFF in processing electronic-grade 2D materials at industrial-scale.

Life cycle assessment and technoeconomic analysis

To assess the environmental sustainability improvements for our process, we first conducted a comprehensive life cycle assessment (LCA) comparing the use of ceramic membranes with our previous study employing polymer membranes (Table 1).[19] Additionally, we conducted a comparative techno-economic analysis (TEA) to quantify the economic benefits of our process. Fig. 4(a) depicts the system boundary for both analyses. Using a functional unit of 1 L of graphene ink, we considered the entire ink production process. These results

Table 1 LCA/TEA inventory for the production of 1 L of graphene ink

Input	Unit	Polymer membrane values	Ceramic membrane values
Graphite	g	4.5	76
Ethyl cellulose	g	0	0.05
EtOH	g	0.71	0.20
TpOH	g	0.093	0.093
Glass	g	0.50	0.50
Membranes	g	0.0032	0.00070
Tubing	g	0.0018	0.00060
Electricity	MJ	24	0.34

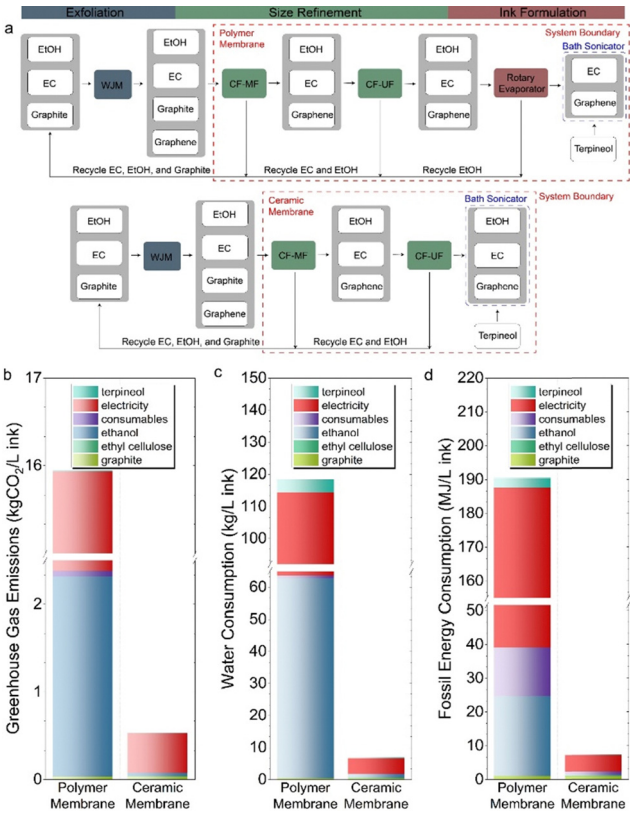

Fig. 4 Life cycle assessment (LCA) using 1 L of graphene ink as a functional unit. (a) Schematic of the graphene ink production process and the LCA system boundary for polymer (top) and ceramic (bottom) membranes. (b)–(d) Greenhouse gas emissions, water consumption, and fossil energy consumption is reduced by 97%, 96%, and 94% respectively, when using ceramic membranes compared to polymer membranes.

thus expand upon the scope of our past work in which CFF with polymer membranes had notable limitations including high capital equipment costs, labor-intensive requirements, and non-trivial energy consumption.[19] With polymer membranes, we assumed that we can recycle all of the ethyl cellulose and ethanol using rotary evaporation, while recovering all of the unexfoliated graphite. With ceramic membranes, we similarly assumed that we can recycle all of the unexfoliated graphite along with the ethyl cellulose present in the graphitic suspension and the ethanol unused to produce the graphene ink. We also completed sensitivity analyses to evaluate the effect of membrane operation and cleaning on mass throughput (ESI†).

The resulting LCA calculations reveal that the implementation of ceramic membranes in an integrated CF-MF/CF-UF process to produce graphene inks reduces greenhouse gas (GHG) emissions, water consumption, and fossil fuel consumption by 97%, 96%, and 94%, respectively, in comparison to CFF using polymer membranes (Fig. 4(b)–(d), Table 2). Four factors contribute to these improvements. First, when the membrane is polymeric, both CF-MF and CF-UF operate for longer durations because the reduced surface area of the membrane necessitates extended operation. Second, rotary evaporation is not required in the ceramic membrane-based process. The rotary evaporator is energy intensive since it requires a chiller to condense gaseous solvent and a high-vacuum pump to pull gas into the condenser. When a ceramic membrane is used in both the CF-MF and CF-UF processes, the CF-UF permeate can be directly used to produce inks without a rotary evaporation step. Third, ethanol consumption is an order of magnitude lower when ceramic membranes are used because the feed concentration to CF-MF can be increased by 10-fold compared to polymer membranes. Fourth, producing polymer membranes (29 MJ kg^{-1}) is more energy-intensive than producing ceramic membranes (0.79 MJ kg^{-1}).[45]

Since the higher throughput from CFF with ceramic membranes is also likely to imply economic benefits, we directly compared the cost of graphene ink production using ceramic and polymer membranes (Fig. 5). In this TEA evaluation, significant gains are achieved in total specific production costs with ceramic membranes reducing cost by 93% compared to polymer membranes. In particular, per 1 L of graphene ink produced, the ceramic membrane process saves $$195 per L or $$738 per gallon at scale. Further analysis of the amortized capital cost, consumables, electricity, and labor required for both processes (Table 3) revealed a cost reduction of 97%. We note that these costs were calculated in $$ per year, so we divided the unit by the respective graphene throughput (g of graphene per year) to obtain $$ per g of graphene, enabling a direct comparison to previous work.[19] Afterwards, we took the

Table 2 Gross environmental impacts per 1 L of graphene ink *via* cross-flow filtration with different membrane materials

	Graphite	EC	EtOH[a]	TpOH[a]	Consumables	Electricity	Total
Greenhouse gas emissions (kg CO_2e per L ink)							
Polymer	0.035	0	2.3	0.010	0.060	13	16
Ceramic	0.035	0.0022	0.040	0.0010	0.0020	0.45	0.53
Fossil fuels (MJ L^{-1} ink)							
Polymer	1.1	0	24	2.9	14	148	191
Ceramic	1.1	0.050	0.40	0.17	0.84	4.9	7.5
Water consumption (kg L^{-1} ink)							
Polymer	0.41	0	63	4.0	0.84	51	119
Ceramic	0.41	0.17	1.05	0.24	0.17	4.9	6.9

[a] Here, EtOH corresponds to ethanol and TpOH corresponds to terpineol.

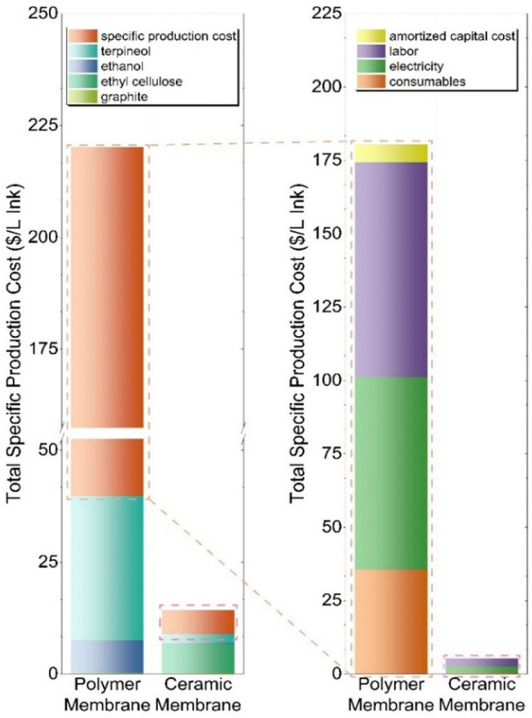

Fig. 5 Technoeconomic analysis (TEA) for ceramic membranes compared to polymer membranes using 1 L of graphene ink as a functional unit.

Table 3 Gross technoeconomic impacts ($) per 1 L of graphene ink

	TEA ($ per L of graphene ink)					
	Graphite	EC	EtOH	TpOH	SPC[a]	Total
Polymer membrane	0.23	0	7.3	32	180	220
Ceramic membrane	0.23	6.6	0.12	1.9	5.44	14

[a] Here, SPC corresponds to specific production cost.

product of $ per g of graphene and the concentration necessary to produce one liter of ink (10 g graphene per L).

The primary driver for the 97% cost reduction in the ceramic membrane process is the improvement in mass throughput; specifically, the CF-MF permeate/CF-UF retentate has significantly greater graphene concentration compared to the CF-MF permeate from the polymer membrane process (Table S5, ESI†). Moreover, producing the required 10 g of graphene per L of ink necessitates considerable resources in the polymer membrane CFF process (*i.e.*, ethanol, electricity, and labor). Additional sensitivity analyses were considered, such as the effect of fouling, increased run time, and labor, which are discussed in length in the ESI.†

Scaling cross-flow filtration with ceramic membranes towards industrial levels may introduce challenges from membrane fouling, which can reduce efficiency and increase maintenance costs. To mitigate these challenges, ceramic membranes can be regenerated while additional membranes are used for separation, a process that can be repeated with multiple membranes operating simultaneously. As a result, ceramic membranes consistently outperform polymer membranes with regard to both environmental sustainability and cost, further reaffirming the benefits of ceramic membrane CFF for the production of electronic-grade graphene inks.

Conclusions

A major limitation of previous CFF processes for solution-processed 2D materials has been the utilization of polymer membranes, which require low feed and permeate concentrations that limit the overall mass throughput. To overcome this limitation, we utilized porous ceramic membranes whose higher mechanical integrity enable high-flow and high-concentration processing for graphene ink production. Ceramic membranes further allow the integration of CF-MF and CF-UF to establish a fully flow-based, direct exfoliation-to-print process for electronic-grade graphene inks. The resulting process produces monodisperse graphene nanosheets with superlative percolating film conductivities of 4×10^4 S m^{-1}. Moreover, the CF-UF retentate, with concentrations ranging from 10^1 to 10^2 g L^{-1}, can be directly combined with terpineol to produce graphene inks compatible with AJP. The resulting inks meet or exceed the performance of centrifugally produced inks and films as confirmed by AFM, SEM, Raman spectroscopy, and charge transport measurements. The incorporation of ceramic membranes in the CFF process leads to substantial improvements in environmental sustainability and cost with LCA and TEA revealing 97%, 96%, 94%, and 93% reductions for greenhouse gas emissions, water consumption, fossil fuel consumption, and specific production costs, respectively. Overall, this work establishes ceramic CFF as an environmentally sustainable and cost-effective separation method for solution-processed 2D materials.

Author contributions

S. D.-A., J. R. D., and M. C. H. conceived the overarching concept. S. D.-A., J. R. D., D. T., J. H., and L. E. C. designed the experiments, performed data measurements, and analyzed the data. S. D.-A., J. T., and J. B. D. performed the life cycle analysis. K. D. and N. A. provided input for the choice of ceramic membranes. All authors discussed the results and commented on the manuscript.

Data availability

Data for this article will be made available *via* the **N**orthwestern MRSEC Da**TA** **R**etrieval (**NECTAR**) at **https://nroads.northwestern.edu/nectar/content/index**.

Conflicts of interest

There are no conflicts to declare.

Acknowledgements

This work was primarily supported by the National Science Foundation (NSF) through the MADE-PUBLIC Future Manufacturing Program (NSF Award Number CMMI-2037026). Additional support for the aerosol jet printing was provided by the U.S. Department of Commerce, National Institute of Standards and Technology (Award No. 70NANB19H005) as part of the Center for Hierarchical Materials Design (CHiMaD). S. D.-A. also acknowledges the National Consortium for Graduate Degrees for Minorities in Engineering and Science (GEM) Fellowship co-administered by Corning Incorporated and Northwestern University. This work utilized the Keck-II, Scanned Probe Imaging and Development (SPID), and Electron Probe Imaging Center (EPIC) facilities of the Northwestern University Atomic and Nanoscale Characterization Experimental (NUANCE) Center, which is supported by the Soft and Hybrid Nanotechnology Experimental (SHyNE) Resource (NSF ECCS-2025633), the Northwestern University Materials Research Science and Engineering Center (MRSEC) program (NSF DMR-2308691), and the International Institute for Nanotechnology (IIN). This work also used the MatCI Facility at Northwestern University, which is supported by the Northwestern University MRSEC (NSF DMR-2308691). Finally, we acknowledge Maryam Khalaj for helpful discussions and Mark A. Jedlicki for his contributions towards the plumbing and integration of the CFF process.

Notes and references

1 L. Yang, W. Chen, Q. Yu and B. Liu, *Nano Res.*, 2020, **14**, 1583–1597.
2 V. Georgakilas, M. Otyepka, A. B. Bourlinos, V. Chandra, N. Kim, K. C. Kemp, P. Hobza, R. Zboril and S. K. Kim, *Chem. Rev.*, 2012, **112**, 6156–6214.
3 H. Bai, C. Li and G. Shi, *Adv. Mater.*, 2011, **23**, 1089–1115.
4 T. Dong, J. Simões and Z. Yang, *Adv. Mater. Interfaces*, 2020, **7**, 1901657.
5 K. P. Lee, T. C. Arnot and D. Mattia, *J. Membr. Sci.*, 2011, **370**, 1–22.
6 I. Pafylias, M. Cheryan, M. A. Mehaia and N. Saglam, *Food Res. Int.*, 1996, **29**, 141–146.
7 M. C. Almécija, R. Ibáñez, A. Guadix and E. M. Guadix, *J. Membr. Sci.*, 2007, **288**, 28–35.
8 Y. Li, J. Luo and Y. Wan, *J. Membr. Sci.*, 2020, **612**, 118432.
9 L. Lin, H. Peng and Z. Liu, *Nat. Mater.*, 2019, **18**, 520–524.
10 K. S. Novoselov, *Science*, 2004, **306**, 666–669.
11 X. Huang, X. Qi, F. Boey and H. Zhang, *Chem. Soc. Rev.*, 2012, **41**, 666–686.
12 S. Bae, H. Kim, Y. Lee, X. Xu, J.-S. Park, Y. Zheng, J. Balakrishnan, T. Lei, H. R. Kim, Y. I. Song, Y.-J. Kim, K. S. Kim, B. Ozyilmaz, J.-H. Ahn, B. H. Hong and S. Iijima, *Nat. Nanotechnol.*, 2010, **5**, 574–578.
13 W. Ren and H.-M. Cheng, *Nat. Nanotechnol.*, 2014, **9**, 726–730.
14 K. L. Ng, B. M. Maciejewska, L. Qin, C. Johnston, J. Barrio, M.-M. Titirici, I. Tzanakis, D. G. Eskin, K. Porfyrakis, J. Mi and N. Grobert, *ACS Sustainable Chem. Eng.*, 2022, **11**, 58–66.
15 W. Kong, H. Kum, S.-H. Bae, J. Shim, H. Kim, L. Kong, Y. Meng, K. Wang, C. Kim and J. Kim, *Nat. Nanotechnol.*, 2019, **14**, 927–938.
16 K. R. Paton, E. Varrla, C. Backes, R. J. Smith, U. Khan, A. O'Neill, C. Boland, M. Lotya, O. M. Istrate, P. King, T. Higgins, S. Barwich, P. May, P. Puczkarski, I. Ahmed, M. Moebius, H. Pettersson, E. Long, J. Coelho, S. E. O'Brien, E. K. McGuire, B. M. Sanchez, G. S. Duesberg, N. McEvoy, T. J. Pennycook, C. Downing, A. Crossley, V. Nicolosi and J. N. Coleman, *Nat. Mater.*, 2014, **13**, 624–630.
17 A. E. Del Rio Castillo, V. Pellegrini, A. Ansaldo, F. Ricciardella, H. Sun, L. Marasco, J. Buha, Z. Dang, L. Gagliani, E. Lago, N. Curreli, S. Gentiluomo, F. Palazon, M. Prato, R. Oropesa-Nuñez, P. S. Toth, E. Mantero, M. Crugliano, A. Gamucci, A. Tomadin, M. Polini and F. Bonaccorso, *Mater. Horiz.*, 2018, **5**, 890–904.
18 X. Cai, Y. Luo, B. Liu and H.-M. Cheng, *Chem. Soc. Rev.*, 2018, **47**, 6224–6266.
19 J. R. Downing, S. Diaz-Arauzo, L. E. Chaney, D. Tsai, J. Hui, J. T. Seo, D. R. Cohen, M. Dango, J. Zhang, N. X. Williams, J. H. Qian, J. B. Dunn and M. C. Hersam, *Adv. Mater.*, 2023, **35**, 2212042.
20 C. Charcosset, *Food Eng. Rev.*, 2020, **13**, 322–343.
21 J. F. Richardson and J. H. Harker, *Chemical Engineering, Particle Technology and Separation Processes*, Butterworth-Heinemann, 2002, vol. 2.
22 G. Belfort, R. H. Davis and A. L. Zydney, *J. Membr. Sci.*, 1994, **96**, 1–58.
23 C. Li, Y. Guo, L. Shen, C. Ji and N. Bao, *Chem. Eng. Sci.*, 2019, **200**, 127–137.
24 Y. Shi, X. Ye, L. Shen and N. Bao, *Chem. Eng. Sci.*, 2022, **248**, 117143.
25 J. C. Trefry, J. L. Monahan, K. M. Weaver, A. J. Meyerhoefer, M. M. Markopolous, Z. S. Arnold, D. P. Wooley and I. E. Pavel, *J. Am. Chem. Soc.*, 2010, **132**, 10970–10972.
26 S. F. Sweeney, G. H. Woehrle and J. E. Hutchison, *J. Am. Chem. Soc.*, 2006, **128**, 3190–3197.
27 S.-G. Yim, Y. Kim, Y.-E. Kang, B. Moon, E. Jung and S. Yang, *Nanomaterials*, 2018, **8**, 959.
28 S. Ohmori, T. Saito, B. Shukla, M. Yumura and S. Iijima, *ACS Nano*, 2010, **4**, 3606–3610.
29 K. C. Pradel, K. Sohn and J. Huang, *Angew. Chem., Int. Ed.*, 2011, **50**, 3412–3416.
30 H. A. Loh, A. Graves, C. D. Stinespring and N. Wu, *ACS Appl. Nano Mater.*, 2019, **2**, 4104–4112.
31 E. B. Secor, J. C. Smith, T. J. Marks and M. C. Hersam, *ACS Appl. Mater. Interfaces*, 2016, **8**, 17428–17434.
32 J.-W. T. Seo, J. Zhu, V. K. Sangwan, E. B. Secor, S. G. Wallace and M. C. Hersam, *ACS Appl. Mater. Interfaces*, 2019, **11**, 5675–5681.
33 K. Parate, S. V. Rangnekar, D. Jing, D. L. Mendivelso-Perez, S. Ding, E. B. Secor, E. A. Smith, J. M. Hostetter, M. C. Hersam and J. C. Claussen, *ACS Appl. Mater. Interfaces*, 2020, **12**, 8592–8603.
34 L. Kuo, V. K. Sangwan, S. V. Rangnekar, T. Chu, D. Lam, Z. Zhu, L. J. Richter, R. Li, B. M. Szydłowska, J. R. Downing,

B. J. Luijten, L. J. Lauhon and M. C. Hersam, *Adv. Mater.*, 2022, **34**, 2203772.

35 International Organization for Standardization, ISO 14040: 2006 Environmental Management—Life Cycle Assessment—Principles and Framework, **https://www.iso.org/standard/37456.html** (accessed July 2023).

36 International Organization for Standardization, ISO 14044: 2006 Environmental Management—Life Cycle Assessment—Requirements and Guidelines, **https://www.iso.org/standard/38498.html**, (accessed July 2023).

37 J. Qin, C. Pei, C. Zhao, Z. Lu, G. Sun and J. Gong, *ACS Sustainable Chem. Eng.*, 2022, **10**, 6999–7009.

38 R. Davis, *Sep. Purif. Rev.*, 1992, **21**, 75–126.

39 W. J. Hyun, E. B. Secor, M. C. Hersam, C. D. Frisbie and L. F. Francis, *Adv. Mater.*, 2014, **27**, 109–115.

40 E. B. Secor, T. Z. Gao, A. E. Islam, R. Rao, S. G. Wallace, J. Zhu, K. W. Putz, B. Maruyama and M. C. Hersam, *Chem. Mater.*, 2017, **29**, 2332–2340.

41 A. C. Ferrari, *Solid State Commun.*, 2007, **143**, 47–57.

42 W. Gao, L. B. Alemany, L. Ci and P. M. Ajayan, *Nat. Chem.*, 2009, **1**, 403–408.

43 A. A. Green and M. C. Hersam, *Nano Lett.*, 2009, **9**, 4031–4036.

44 C. Backes, T. M. Higgins, A. Kelly, C. Boland, A. Harvey, D. Hanlon and J. N. Coleman, Guidelines for Exfoliation, Characterization and Processing of Layered Materials Produced by Liquid Exfoliation, *Chem. Mater.*, 2017, **29**, 243–255.

45 Argonne National Laboratory. GREET 2020. **https://greet.es.anl.gov/index.php** (accessed July 2023).